



IPMC bending predicted by the circuit and viscoelastic models considering individual influence of Faradaic and non-Faradaic currents on the bending



Kota Ikeda^a, Minoru Sasaki^b, Hirohisa Tamagawa^{b,*}

^a Graduate School of Advanced Mathematical Sciences, Meiji University, 4-21-1, Nakano, Nakano-ku, Tokyo, 165-8525, Japan

^b Department of Human and Information Systems, Faculty of Engineering, Gifu University, 1-1 Yanagido, Gifu, Gifu, 501-1193, Japan

ARTICLE INFO

Article history:

Received 25 July 2013

Received in revised form 3 September 2013

Accepted 4 September 2013

Available online xxx

Keywords:

IPMC

Circuit model

Viscoelasticity

Faradaic

Non-Faradaic

ABSTRACT

Electrically induced bending behavior of a highly dehydrated Selemion CMV-based IPMC was analyzed theoretically. The experimental observation suggested that even the highly dehydrated IPMC bending was under the influence of not only Faradaic current but also non-Faradaic current. Hence, it was essential to know the Faradaic and non-Faradaic current influences on the IPMC bending separately for predicting the IPMC bending behavior. A circuit model was proposed for deriving the time-dependent behavior of charge, which was caused by both Faradaic and non-Faradaic currents, passing through the IPMC. In the course of derivation of the time dependence of charge, electrical properties of the IPMC such as resistance and capacitance were obtained, and those physical quantities were reasonable from the stand point of physical chemistry. The time dependent charge behaviors obtained by employing the circuit model successfully resulted in the prediction of bending behavior of the IPMC. The electric properties obtained by the analysis of circuit model was combined with a viscoelastic model we proposed for predicting the bending behavior of IPMC, and the newly proposed viscoelastic model successfully reproduced the experimentally observed behavior of Selemion CMV-based IPMC bending.

© 2013 Elsevier B.V. All rights reserved.

1. Introduction

IPMC (Ionic Polymer Metal Composite) has been widely investigated for the purpose of fabricating a practical bending mode polymer-based actuator [1–6]. IPMC is electrically activated in highly hydrated state. So, the IPMC can be activated even in an aqueous solution unlike other type of actuators, and it is one of IPMCs' featuring facets. Despite intensive efforts made by a number of researchers toward the ultimate research goal of fabricating a practical bending mode actuator of IPMC, the research progress is stagnant recently. There are some challenging tasks to achieve for fabricating a practically utilizable IPMC. The IPMC has to be able to generate higher force and has to exhibit more precisely controllable bending behavior.

The IPMC is usually electrically activated in highly hydrated state. It has been firmly believed that the bending of IPMC is due to the shift of mobile hydrated ions inside the IPMC under applied voltage [7,8]. This means that a large quantity of water is needed for inducing the bending of IPMC. Contrary to that bending mechanism firmly believed and accepted, however, it was found that one

of IPMCs consisting of a Selemion CMV coated with silver exhibited relatively large bending under applied voltage even in the highly dehydrated state [9–12], (Selemion CMV is an ion exchange membrane containing $-\text{SO}_3\text{H}$ functional atomic groups, manufactured by Asahi Glass Co., Ltd., Tokyo, Japan). A completely dehydrated Selemion CMV-based IPMC cannot exhibit bending because of the loss of electrical conductivity, however, highly dehydrated (not-completely dehydrated) Selemion CMV-based IPMC can exhibit large bending with improved bending controllability [9]. Nafion is one of ion exchange membranes, whose chemical structure is quite similar to Selemion CMV. It was found that Nafion-based IPMC (Nafion coated with silver) exhibited bending under applied voltage, too, even in the highly dehydrated state, though its bending curvature was quite small [13]. Furthermore, the Nafion-based IPMC bending controllability was largely improved in the highly dehydrated state compared with that in hydrated state. According to the experimental facts so far described, the dehydration treatment to the Selemion CMV-based IPMC and Nafion-based IPMC improved their bending controllability. Therefore, we have thought that minimizing the occurrence of non-Faradaic current in the IPMC body resulted in the improvement of IPMC bending controllability. However, our current study revealed that even the highly dehydrated IPMC is under heavy influence by the non-Faradaic current. Because of the importance of precise controllability for

* Corresponding author. Tel.: +81 582932529; fax: +81 582932529.

E-mail address: tmgwhrhs@gifu-u.ac.jp (H. Tamagawa).

a practical IPMC actuator, we attempted to elucidate the roles of non-Faradaic current as well as Faradaic current for the IPMC bending controllability. First, we proposed a circuit model of the highly dehydrated IPMC and derived its electrical properties such as its resistance, capacitance and etc. Then the bending behavior of Selemion CMV-based IPMC was predicted. We moved onto the next step: by employing those electrical properties derived in the circuit model, we investigated the bending behavior of the same Selemion CMV-based IPMC from the stand point of elasticity and successfully predicted its bending behavior.

2. Circuit model

2.1. Experiment

To begin with, we would like to explain the essential conditions for building a circuit model of the Selemion CMV-based IPMC, then we introduce a circuit model. Hence, above all, we experimentally studied the bending behavior of Selemion CMV-based IPMC.

A Selemion CMV-based IPMC was fabricated simply by coating a Selemion CMV surface with silver by the silver mirror reaction [14]. The resultant Selemion CMV-based IPMC was dehydrated by storing it in a desiccator with desiccant, resulting in a highly dehydrated (not-completely dehydrated) Selemion CMV-based IPMC. It was cut into a strip of $20\text{ mm} \times 2\text{ mm} \times 120\text{ }\mu\text{m}$ (hereafter the strip is called CMV IPMC). One end of the CMV IPMC was horizontally clamped with a pair of electrodes as illustrated at upper part in Fig. 1(a). By using this experimental setup, we carried out the following bending testing of CMV IPMC (see the CMV IPMC in the bent state as illustrated at the lower part in Fig. 1(a)): 1.5 V constant voltage was applied on the CMV IPMC from time $t=0\text{ s}$ to 20 s, and subsequently its top and bottom surfaces were short-circuited with a resistor as illustrated in Fig. 1(b). During the 1.5 V voltage application process for the initial 20 s, vertical displacement of the CMV IPMC surface 10 mm away from its clamping point was measured with a laser displacement sensor as a function of time, as illustrated in Fig. 1(a). The measured vertical displacement was later converted into curvature. Simultaneously, the current was measured as a function of time. Definitions of the positive and negative

direction of the curvature and current are shown in Fig. 1(a). When the top and bottom surfaces of CMV IPMC were short-circuited after the 1.5 V voltage application process, the current flowing through the $10\text{ }\Omega$ -resistor of r was measured as a function of time, where the definition of the positive and negative of current is shown in Fig. 1(b). At the same time, the vertical displacement of the CMV IPMC surface 10 mm away from its clamping point was measured with a laser displacement sensor as a function of time. Fig. 2(a) shows the time dependence of current, when the voltage application and short-circuit tests were carried out, where the thick curve represents the current induced under voltage application of 1.5 V and the fine curve represents the current flowing through the resistor when short-circuited.

Absolute humidity (AH) is quite substantial factor for determining the bending behavior of IPMC in response to external electric stimulation. All the experimental measurements shown in this paper were all carried out at the low absolute humidity of $\text{AH} \sim 9\text{ gm}^{-3}$. Unexpectedly, Fig. 2(a) suggests that even highly dehydrated CMV IPMC exhibited the discharge of non-negligible quantity of charge from $t=20\text{ s}$. The charge was stored in the CMV IPMC in the middle of 1.5 V voltage application, and it was relatively large quantity of charge compared with the charge imposed on the CMV IPMC from $t=0\text{ s}$ to 20 s. Fig. 2(b) shows the relationship between the total charge induced from $t=0\text{ s}$ and the CMV IPMC bending curvature. Thick curve represents the CMV IPMC bending curvature vs. total charge induced under voltage application of 1.5 V. Fine curve represents the CMV IPMC bending curvature vs. the sum of the charge induced from $t=0\text{ s}$ to 20 s under 1.5 V and the charge flowing through the resistor r from $t=20\text{ s}$ onward by the discharging process. What is quite intriguing about Fig. 2(b) is that the decay of the bending curvature was induced when discharged. Furthermore, we noticed that the bending curvature in the decaying process did not trace back its trajectory from $t=0\text{ s}$ to 20 s.

We carried out another experiment. A voltage increasing at the rate of 10 mVs^{-1} from 0 V to 1.5 V was applied on a CMV IPMC and its current and curvature were measured. Fig. 3 shows voltage dependence of current flowing through the unit surface area of the CMV IPMC and the voltage dependence of CMV IPMC curvature. It is noticeable that the current and the curvature started increasing

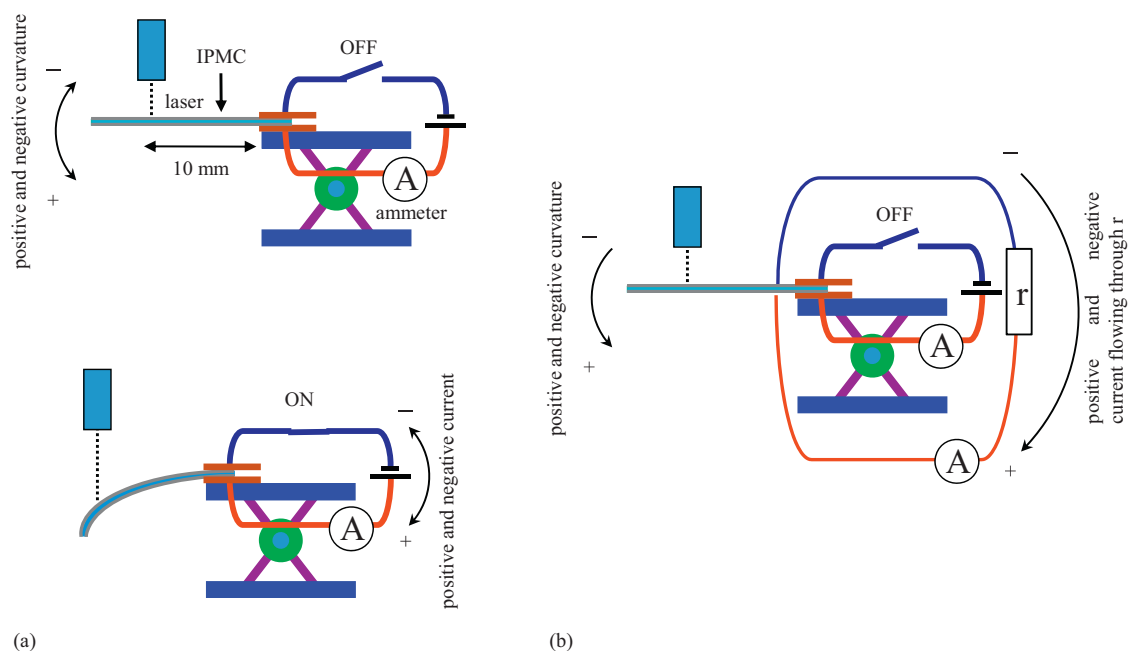


Fig. 1. (a) A CMV IPMC set to the bending testing apparatus at ON and OFF stages. (b) The CMV IPMC, when short-circuited with a $10\text{ }\Omega$ resistor.

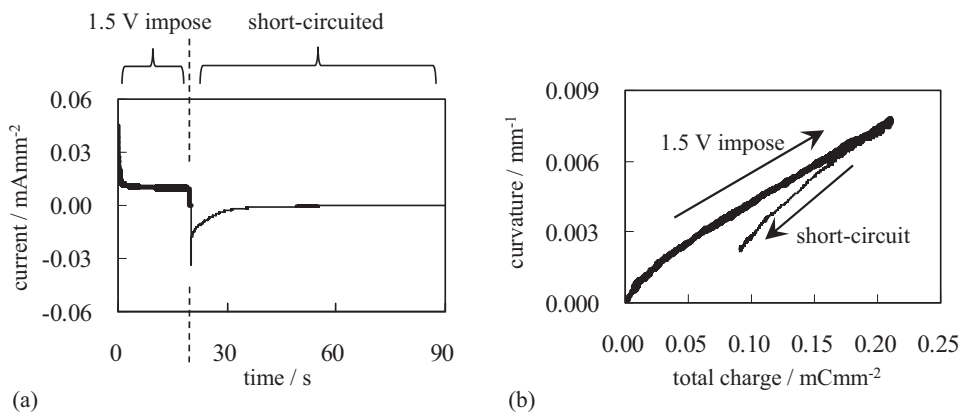


Fig. 2. (a) Time dependence of current, where the thick curve represents the current induced under voltage application of 1.5 V and the fine curve represents the current flowing through the resistor when short-circuited. (b) CMV IPMC bending curvature vs. total charge imposed. Thick curve represents the CMV IPMC bending curvature vs. total charge induced under voltage application of 1.5 V. Fine curve represents the CMV IPMC bending curvature vs. the sum of the charge flowing through the CMV IPMC from $t = 0$ s to 20 s and another charge flowing through the $10\text{-}\Omega$ -resistor r from $t = 20$ s onward.

around at 0.7 V as indicated by a dashed arrow in Fig. 3. As already reported for the past several years, redox reaction of $\text{Ag} \leftrightarrow \text{Ag}_2\text{O}$ starts around above 0.7 V, that is, 0.7 V is threshold voltage for the induction of redox reaction [11]. Effective bending of CMV IPMC and effective current induction were always simultaneously observed and they were inevitably accompanied by the redox reaction of $\text{Ag} \leftrightarrow \text{Ag}_2\text{O}$. Ag on the anode was oxidized and Ag_2O on the cathode was reduced. Polarity change of voltage caused opposite reaction, hence, it is reversible redox reaction. CMV IPMC bending, current induction and redox reaction are undoubtedly intimately correlated one another.

Next, we investigated the surface color change behavior of CMV IPMC in response to the polarity change of applied voltage. Fig. 4 shows the relationship among CMV IPMC bending direction, voltage polarity and redox reaction (surface color change of CMV IPMC). Initially as shown in Fig. 4(a), both top and bottom surfaces of CMV IPMC were bright because of white Ag color. Once the 1.5 V voltage was imposed, bottom surface (anode surface) darkened due to the creation of Ag_2O as shown in Fig. 4(b). Then the discharging by connecting the top and the bottom surfaces with a resistor caused backward bending of CMV IPMC and reduction of Ag_2O into Ag on the bottom surface, and the oxidation of Ag on the top surface into Ag_2O was also induced, as shown in Fig. 4(c). Of course these two reactions were induced simultaneously.

2.2. Building a circuit model

What is so far described brought us some essential requirements for building an appropriate circuit model explaining CMV IPMC bending behavior. Those essential requirements are given below:

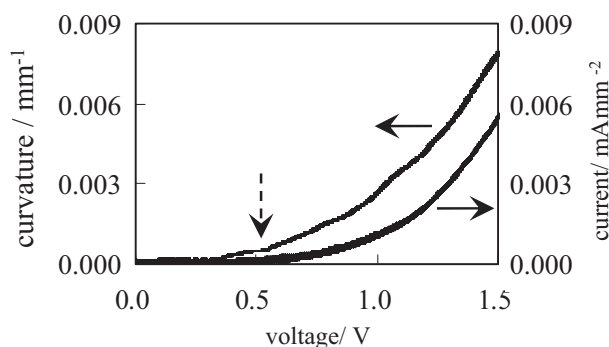


Fig. 3. CMV IPMC bending curvature vs. voltage imposed, and current flowing through the CMV IPMC vs. voltage imposed.

- (i) As shown in Fig. 2(a), the CMV IPMC can store a certain quantity of charge.
- (ii) As shown in Figs. 2(b) and 3, increase and decrease of charge or current has decisive role for the increase and decrease of bending curvature of CMV IPMC, respectively.
- (iii) Effective redox reaction of $\text{Ag} \leftrightarrow \text{Ag}_2\text{O}$ is induced around at or above 0.7 V applied voltage as shown in Fig. 3.
- (iv) Below at 0.7 V, the redox reaction is not induced effectively, but a small current can flow through CMV IPMC. That current is ineffective for the induction of CMV IPMC bending as shown in Fig. 3.
- (v) Even discharging process can cause the redox reaction of $\text{Ag} \leftrightarrow \text{Ag}_2\text{O}$ as shown in Fig. 4.

As the circuit model has to satisfy the above five requirements, we propose a circuit model illustrated in Fig. 5(a) with the comments (a)–(d) below that explain further our proposal.

- (a) Selemion CMV part of the CMV IPMC is approximated by a capacitor C_ℓ and a resistor R . Since C_ℓ can store a certain quantity of charge, the requirement (i) is satisfied, where we will denote the capacitance of C_ℓ and resistance of R by C_ℓ and R , respectively. Silver layers are approximated by r_ℓ , where its resistance is denoted by r_ℓ , too. Although there are two silver layers on the surfaces of CMV IPMC, both surface resistances are combined into one, r_ℓ . We hypothesized that charge storage in the capacitor C_ℓ induces the CMV IPMC bending. It is the bending induced by non-Faradaic current, and also we hypothesized that the occurrence of current I_r (see Fig. 5(a)) flowing through the resistor r_ℓ inevitably causes the redox reaction, resulting in the induction of bending. It is the bending induced by Faradaic current. It was hypothesized that the downward bending of CMV IPMC was induced, when $Q_\ell > 0$ or $I_r > 0$, where Q_ℓ is the charge stored in C_ℓ (see Fig. 5(a)).
- (b) Since it has been reported occasionally that the curvature of highly dehydrated silver-plated Selemion CMV IPMC (virtually the same as the CMV IPMC) is proportional to the total charge imposed on it, we further hypothesized that the curvature proportional to Q_ℓ and another curvature proportional to the total charge passing through r_ℓ could be induced. So, what is described about C_ℓ and r_ℓ here satisfies the requirement (ii).
- (c) Another capacitor C_s and resistor r_s were introduced into the circuit model relating to the (iii) and (iv), where the capacitance of C_s and resistance of r_s are denoted by C_s and r_s , respectively. We hypothesized that the current flowing through C_s and r_s cannot cause any bending of CMV IPMC. Namely, this

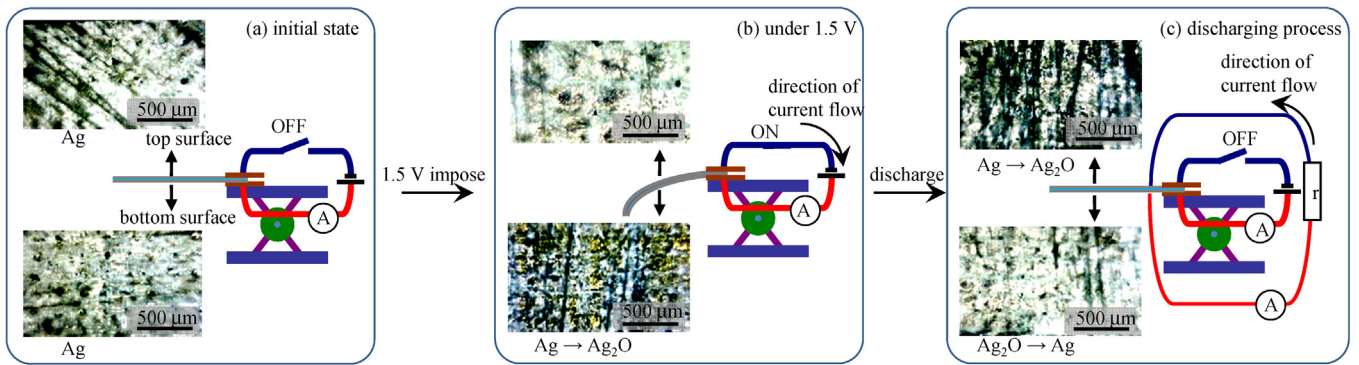


Fig. 4. The relationship between CMV IPMC bending direction, voltage polarity and redox reaction (surface color change of CMV IPMC).

capacitance and resistor is a model of the path for the experimentally observed current causing ineffective bending of CMV IPMC below 0.7V shown in Fig. 3. Since effective bending of CMV IPMC was not induced up to 0.7V, most of the current must flow through this path and the total charge induced up to 0.7V was quite small compared with that at or above 0.7V, we hypothesized that both C_s and r_s were quite small. We the authors would like to urge the reader to firmly bear in mind that C_s and r_s are just a path for a current causing no bending in this circuit model, and only the charge stored in C_ℓ and the charge flowing through r_ℓ can cause the CMV IPMC bending.

(d) Now imagine that the voltage of 1.5 V was applied on CMV IPMC and subsequently discharging was carried out. When in the discharging process, the direction of current flowing through r_ℓ is reversed as illustrated in Fig. 5(b). Therefore, the redox reaction during discharging process predicted by this circuit model satisfies the requirement (v).

Now, we would like to prove the appropriateness of our circuit model by comparing the model with the experimental evidences. The CMV IPMC is featured especially by the functional atomic groups of $-SO_3H$ contained in it. It comes to contain immobile anions of $-SO_3^-$ and mobile cations of H^+ in the hydrated state (even in the highly dehydrated state unless in the completely dehydrated state) as illustrated in Fig. 6(a). Once the constant voltage 1.5 V is imposed on it, it exhibits downward bending (in the anode direction). This bending process is explained from the stand point of physical chemistry. All cations are shifted toward cathode side of the CMV IPMC. It causes the swelling of cathode side of the CMV IPMC,

and the contraction of the anode side, resulting in the downward bending, as illustrated in Fig. 6(b-1). The state shown in Fig. 6(b-1) is interpreted as the storage of charge Q_ℓ in C_ℓ from the stand point of the circuit model as illustrated in Fig. 6(b-2). The current charging C_ℓ is non-Faradaic current. The experimental observation of CMV IPMC bending by non-Faradaic current is well explained by the circuit model. As described earlier, it was hypothesized that the CMV IPMC bending is caused by Faradaic current as well, inducing the redox reaction of $Ag \leftrightarrow Ag_2O$. In fact, we observed the redox reaction of $Ag \leftrightarrow Ag_2O$ and the bending simultaneously, during the application of 1.5 V on the CMV IPMC. As easily understood, the charge storage (or release) process inevitably causes the current passing through r_ℓ in the circuit model shown in Fig. 6(b-2). The direction of the current I_r passing through r_ℓ is shown in Fig. 6(b-2) and it is known that CMV IPMC exhibits bending in the anode direction, though the mechanism of bending induced by Faradaic current has not been elucidated yet. Hence the circuit model is so far quite consistent with the experimental evidences. We further assessed the validity of our idea that Faradaic and non-Faradaic current have individual influence of inducing IPMC bending by studying another type of IPMC as described below.

Selemion AMV is another type of ion exchange membrane manufactured by ASAHI GLASS Co., Ltd., Tokyo, Japan. Since it is an anion exchange membrane, it contains immobile cations and mobile anions in hydrated state (even in the highly dehydrated state unless in the completely dehydrated state). As easily understood, the electrical structure of Selemion AMV is just the opposite to that of the Selemion CMV. Coating the surface of the Selemion AMV resulted in a Selemion AMV-based IPMC (hereafter called AMV IPMC). Bending

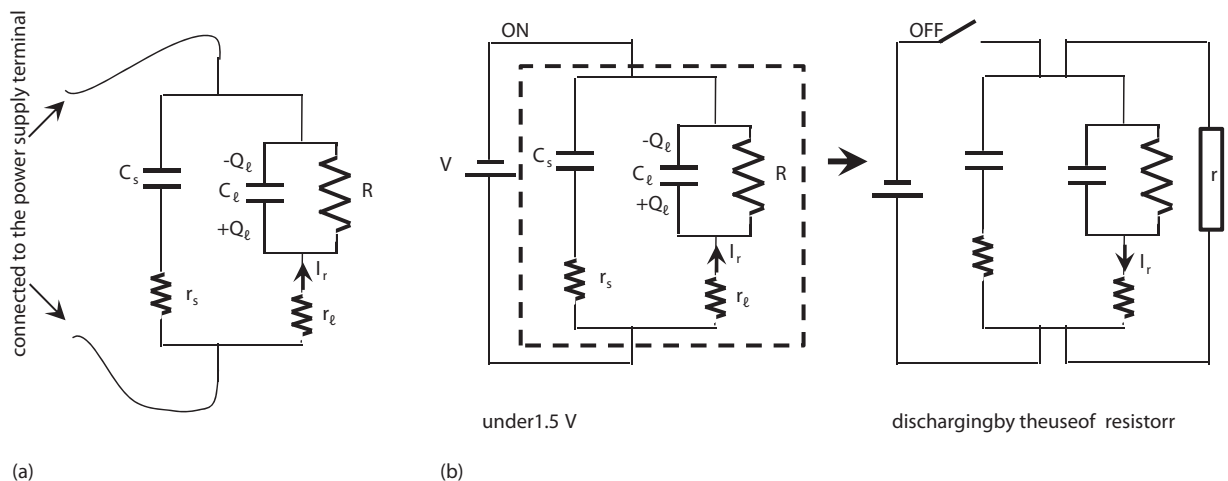


Fig. 5. (a) Circuit model (b) under 1.5 V and in the discharging process.

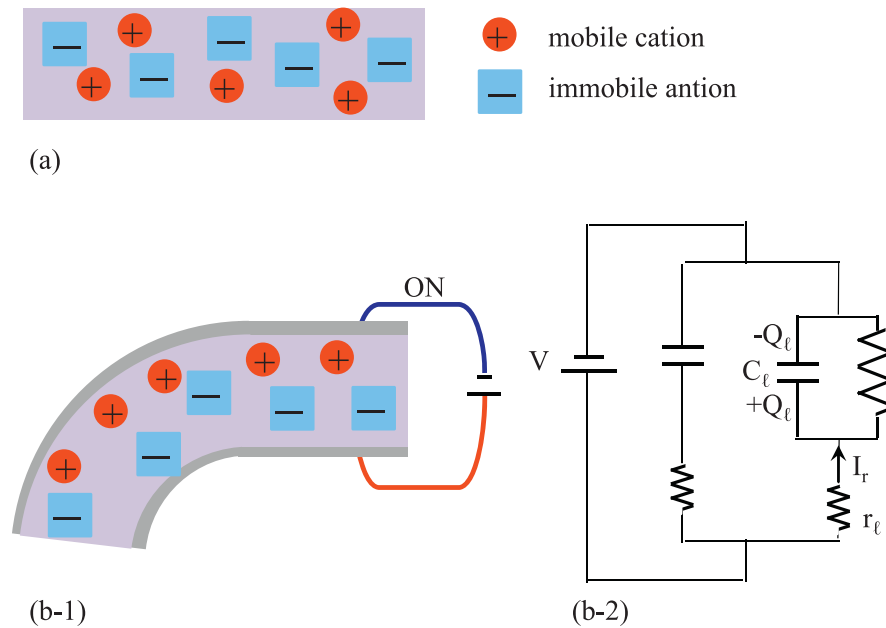


Fig. 6. (a) Selemion CMV in the hydrated state (b-1) bending under applied voltage and shift of mobile cations toward cathode and (b-2) its circuit model.

test of the AMV IPM was carried out by employing the same setup as illustrated in Fig. 1(a). 1.5 V constant voltage was imposed for 180 s on the AMV IPM horizontally clamped with a pair of electrodes and followed by discharging process by connecting its top and bottom surfaces with a resistor (short-circuit). Fig. 7 shows the time dependence of AMV IPM bending curvature. The AMV IPM initially exhibited upward bending (negative curvature). But around at time $t = 30$ s it changed the bending direction downward. This unusual behavior is explained as follows: Once the voltage of 1.5 V was imposed at $t = 0$ s, immediately mobile anions tended to shift downward as illustrated in Fig. 8(a), causing the upward bending of the AMV IPM. While in progress of the upward bending, redox reaction of $\text{Ag} \leftrightarrow \text{Ag}_2\text{O}$ is in progress, too, and gradually the influence of the redox reaction on the induction of AMV IPM bending comes to be dominant. Since the silver plated IPM has tendency to bend in the anode direction by $\text{Ag} \leftrightarrow \text{Ag}_2\text{O}$ redox reaction, the AMV IPM comes to exhibit downward bending around after $t = 30$ s. Long after $t = 30$ s but before starting discharging process at $t = 180$ s,

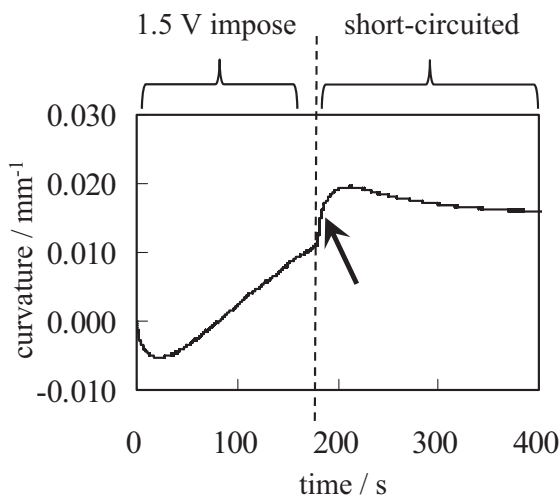


Fig. 7. Time dependence of AMV IPM curvature in the middle of 1.5 V voltage impose followed by discharging.

already the redox reaction was dominant for the induction of AMV IPM bending. Although mobile anions were mostly located at the anode side of the AMV IPM right before $t = 180$ s, and since redox reaction was dominant for the induction of bending as illustrated in Fig. 8(b), the curvature of AMV IPM is positive. Once the discharging process started at $t = 180$ s, all anions were liberated from anode side and tended to homogeneously disperse in the AMV IPM body as illustrated in Fig. 8(c), causing further downward bending as indicated by a solid arrow in Fig. 7. This discharging process causes the redox reaction, too, according to the circuit model (see Fig. 5(b)). During the redox reaction after $t = 180$ s, Ag on the top surface was oxidized into Ag_2O , while the Ag_2O on the bottom surface was reduced into Ag. Therefore, the redox reaction caused in the discharging process has influence of inducing upward bending. Hence, bending relaxation started around at $t = 200$ s as shown in Fig. 7.

Concerning what has been described so far, the circuit model with considering Faradaic and non-Faradaic current appears to well explain the bending behavior of IPMCs.

2.3. Parameter estimate

We hypothesized that the curvature is induced by the charge, Q_F , of Faradaic current passing through the resistor r_ℓ of silver layer and by the another charge, Q_ℓ , of non-Faradaic current stored in the capacitor C_ℓ of Selemion CMV phase. Q_F and Q_ℓ are supposed to induce the curvature B_F and B_{nF} , and B_F and B_{nF} are assumed to be given by Eqs. (2.1) and (2.2), respectively. The total curvature, B , is the sum of B_F and B_{nF} as represented by Eq. (2.3):

$$B_F = k_F Q_F \quad (2.1)$$

Coefficient k_F is determined experimentally.

$$B_{nF} = k_{nF} Q_\ell \quad (2.2)$$

Coefficient k_{nF} is determined experimentally.

$$B = B_F + B_{nF} \quad (2.3)$$

Fig. 9(a) shows the time dependence of CMV IPM curvature under rectangular oscillating voltage with the amplitude = 1.5 V and its frequency = 1/60 Hz. This experimental result is rearranged into curvature vs. charge as shown in Fig. 9(b-1 and 2). The charge was

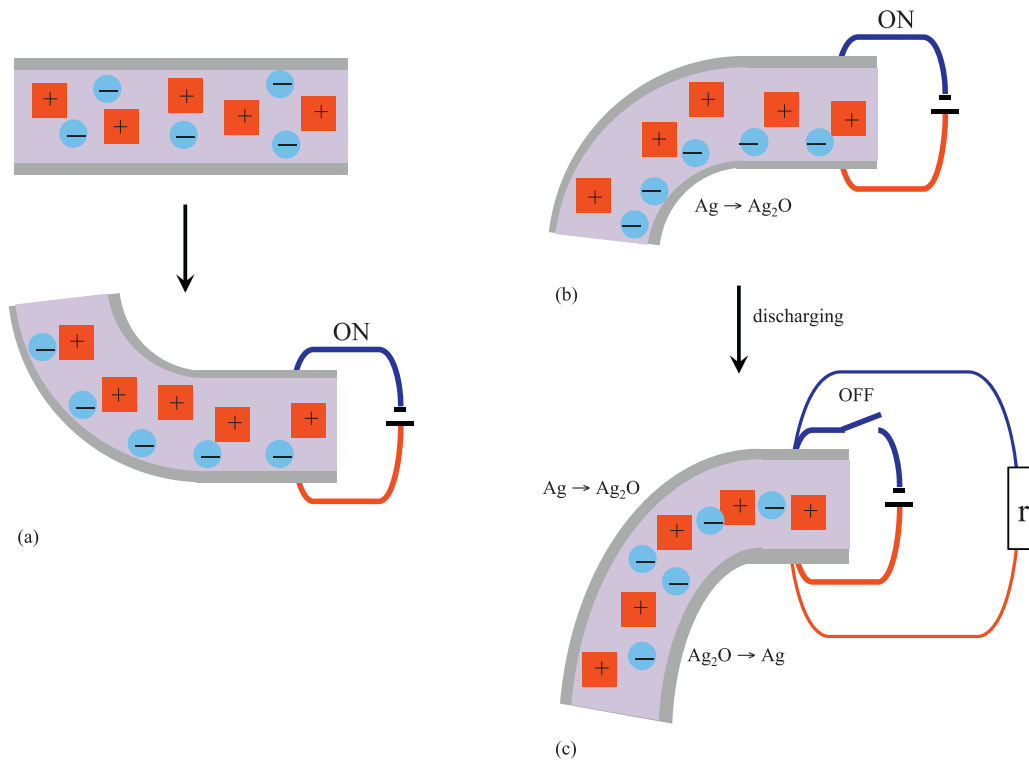


Fig. 8. Explanation of AMV IPMC bending.

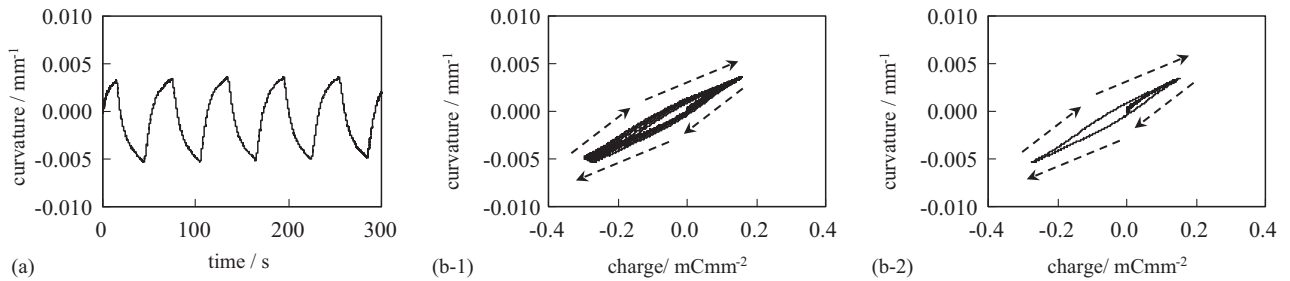


Fig. 9. (a) Time dependence of CMV IPMC curvature under rectangular oscillating voltage (amplitude 1.5 V, frequency 1/60 Hz). (b) Curvature vs. Charge about CMV IPMC (b-1) from $t = 0$ s through 300 s and (b-2) from $t = 0$ s through 75 s, where the dashed arrows represent the progression of time.

measured by the ammeter shown in Fig. 1. This means that the charge shown in Fig. 9(b-1 and 2) is the total charge passing through the whole circuit normalized by the unit surface area of CMV IPMC. We would like to make comment on the Fig. 9(b-1 and 2), where the dashed arrows indicate the progression of time. The diagram forms parallelogram shape trajectory. It is a quite typical behavior between the curvature and charge in case where the CMV IPMC is activated under rectangular oscillating voltage. In order to know the curvature of B_F and B_{nF} , it is necessary to know the Q_f and Q_l . In order to obtain them, it is necessary to estimate the parameters (τ_s , τ_l , Q_s , Q_l , C_s , C_l , r_s , r_l , R) given in Fig. 10, where Q_s represents the charge stored in C_s , and τ_s and τ_l are characteristic time and their exact definitions are given in Eq. (2.1), where $I(t)$ represents the entire current generated by the power supply (see Fig. 10). Derivation procedure of Eq. (2.1) is given in Appendix A.

$$I(t) = \frac{Q_s}{\tau_s} \exp\left(-\frac{t}{\tau_s}\right) + \frac{RC_l - \tau_l}{\tau_l RC_l} Q_l \exp\left(-\frac{t}{\tau_l}\right) + \frac{Q_l}{RC_l} \quad (2.4)$$

where $\tau_s = r_s C_s$, $Q_s = C_s V$, $\tau_l = \frac{C_l r_l R}{r_l + R}$ and $Q_l = \frac{R}{r_l + R} C_l V$.

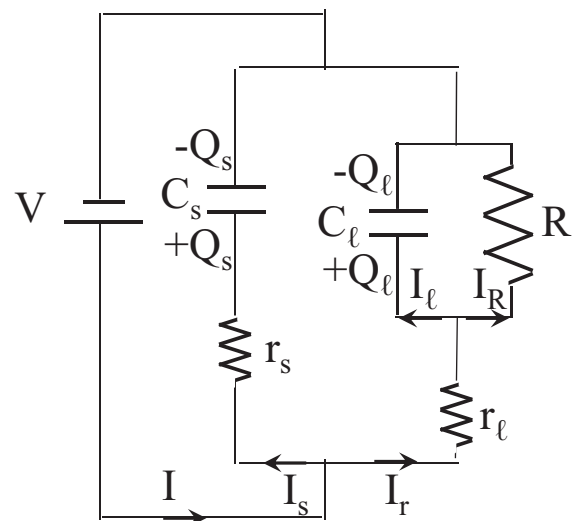


Fig. 10. Circuit model with parameters.

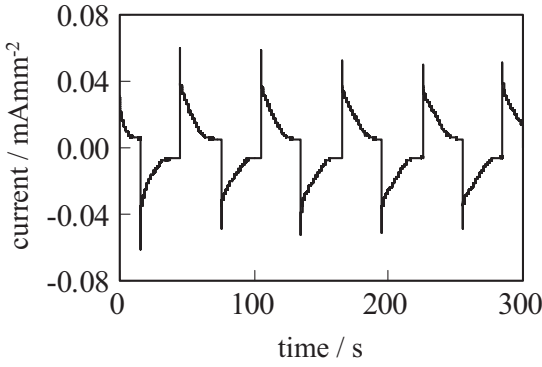


Fig. 11. Time dependence of current induced in the CMV IPMC under rectangular oscillating voltage (amplitude 1.5 V, frequency 1/60 Hz).

Fig. 11 shows the time dependence of current, I , when the experiment for Fig. 9 was carried out. Eq. (2.4) is valid for $t=0$ s through $t=15$ s. By curve fitting technique to the current data from $t=0$ s through 15 s in Fig. 11, all the parameters were determined. But we did not use these parameters for the analysis of CMV IPMC bending behavior. Because empirically we found that the parameters determined by the use of current data for $t=0$ s through 15 s never brought us so appropriate outcomes. Although we have not figured out the exact reason of inappropriateness about the use of parameters obtained by the use of current data for the initial 15 s, we are now close to finding out the reason. It is to be shown in the future report from us. Those parameters were good only for explaining the CMV IPMC bending behavior at early stage. Therefore, those parameters were used only for obtaining Q_s^T and Q_ℓ^T introduced below:

$$Q_s^T \equiv Q_s(t = T) = Q_s \left[1 - \exp\left(-\frac{T}{\tau_s}\right) \right] \quad (2.5)$$

where $V = 1.5$ V and $T = 15$ s.

$$Q_\ell^T \equiv Q_\ell(t = T) = Q_\ell \left[1 - \exp\left(-\frac{T}{\tau_\ell}\right) \right] \quad (2.6)$$

where $V = 1.5$ V and $T = 15$ s.

At time $t = 15$ s, the voltage polarity was reversed and another equations are derived for the circuit, and the $t = 15$ is redefined as $t' = 0$ s. Therefore, Eqs. (2.5) and (2.6) can be respectively regarded as $Q_s(t' = 0)$ and $Q_\ell(t' = 0)$.

Under defining $t = 15$ s as $t' = 0$ s, all the parameters are redefined by placing a prime on the shoulder of individual parameters. Then we derived the entire current generated by the power supply, $I'(t')$, given in Eq. (2.7). Derivation procedure of Eq. (2.7) is given in Appendix B.

$$I'(t') = I'_s(t') + I'_i(t') + I'_R(t') = \frac{Q'_s - Q_s^T}{\tau'_s} \exp\left(-\frac{t'}{\tau'_s}\right) + \frac{(Q'_i - Q_i)(\tau'_i - R'C_i)}{R'C_i\tau'_i} \exp\left(-\frac{t'}{\tau'_i}\right) + \frac{Q'_i}{R'C_i} \quad (2.7)$$

By the curve fitting technique to the current data from $t = 15$ s through 45 s in Fig. 11, all the parameters were finally determined. They are summarized in Table 1. The parameters in Table 1 are to be used for the analysis of CMV IPMC bending behavior.

2.4. Prediction of bending behavior

Now we move on to the process of deriving the k_F and the k_{nF} . We focus on the charge and curvature behavior from $t = 15$ s through 45 s shown in Figs. 9 and 11 and those experimental data were arranged into curvature vs. charge as shown in Fig. 12. Bear

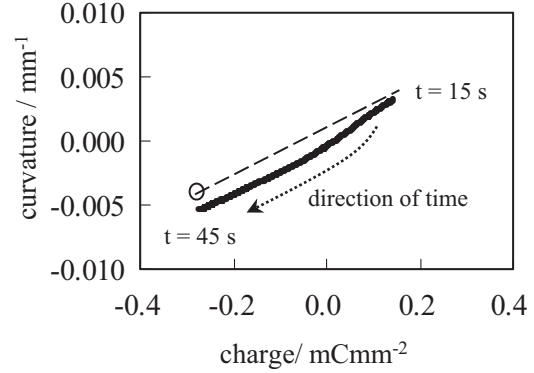


Fig. 12. Curvature vs. Charge about CMV IPMC from $t = 15$ s through $t = 45$ s.

in mind that since the capacitance of C_s is negligibly small compared to that of C_ℓ , the charge shown in Fig. 12 virtually consists of Faradaic current passing through r_ℓ and non-Faradaic current stored in the capacitor C_ℓ . Right before $t = 45$ s in Fig. 12, the curvature change with time was primarily caused by the Faradaic current passing through the silver layer of r_ℓ , since the capacitances C_s and C_ℓ were full of charge. Therefore, the curvature at and right before $t = 45$ s is represented simply by Eq. (2.1), and k_F is given as the gradient of tangential line of curve right before $t = 45$ s in Fig. 12. Dashed line in Fig. 12 has the slope k_F , where the line passes through the data point at $t = 15$ s. This line reaches the point indicated by a circle at $t = 45$ s in Fig. 12. The curvature at the point indicated by the circle is totally different from the experimentally observed curvature at $t = 45$ s. This curvature difference must be caused by the charge stored in the capacitor C_ℓ from $t = 15$ through 45 s. Since it is possible to compute the charge quantity change and the curvature difference between $t = 15$ s and 45 s, k_{nF} is easily obtained based on Eq. (2.2). k_F is 0.0159 mC⁻¹ and k_{nF} is 0.0071 mC⁻¹. By the use of these k_F and k_{nF} and the parameters shown in Table 1, we computed the bending curvature behavior of CMV IPMC under the rectangular oscillating voltage (amplitude 1.5 V, frequency 1/60 Hz). Fig. 13 shows the computed result of the relationship between the CMV IPMC bending curvature and charge from $t = 0$ s through 75 s. This diagram is in good agreement with the experimental data in Fig. 9(b-2).

Researchers have already reported various circuit models of IPMCs for characterizing the electrical and electromechanical properties of IPMCs [15–18]. The circuit model proposed in this paper is one of such models. However, our circuit model is distinct from others, that is, our circuit model takes into consideration the types of currents, Faradic and non-Faradaic currents. Unlike the other models, the influence of Faradic and non-Faradaic currents on the CMV IPMC bending is analyzed individually.

Some may argue that there is nothing meaningful about the results given in Fig. 13, since all the parameters were determined so that the computed result shown in Fig. 13 reproduces the experimental result shown in Fig. 9(b-1) and (b-2). In order to defy such an argument, we performed further analysis of CMV IPMC bending behavior. Using some concept employed in the circuit model, we did an analysis of CMV IPMC bending behavior based on the viscoelasticity. Namely, the bending behavior of CMV IPMC is explained from the standpoint of physics and the circuit model we proposed. It is described in the next section.

3. Viscoelastic analysis

The meaning of our circuit model should be clearly shown here. For the purpose of it, we will attempt to explain the free bending

Table 1
Parameters for the circuit model.

τ_s/s	τ_l/s	$Q_s/mC\text{mm}^{-2}$	$Q_l/mC\text{mm}^{-2}$	$C_s/mF\text{mm}^{-2}$	$C_l/mF\text{mm}^{-2}$	$r_s/k\Omega\text{mm}^2$	$r_l/k\Omega\text{mm}^2$	$R'/k\Omega\text{mm}^2$
0.18	6.7	0.00247	0.202	0.00165	0.168	109.2	49.8	200.2

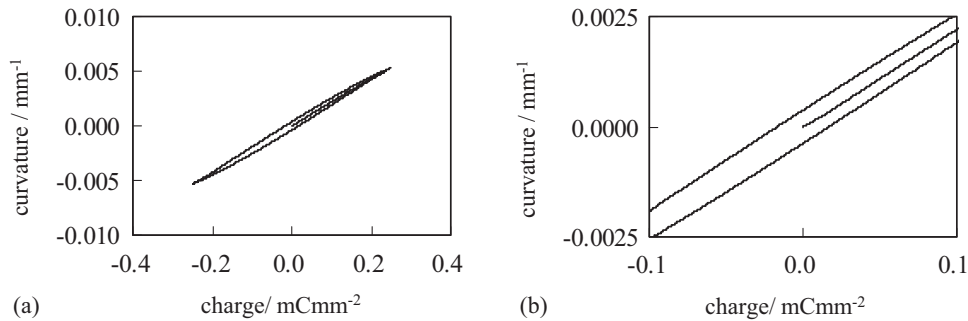


Fig. 13. Curvature vs. Charge predicted by the circuit model about CMV IPMC (b) shows the part of (a) magnified by a factor of around 2.

behavior of a CMV IPMC employing a certain idea from the circuit model. More concretely, we will employ the viscoelastic theory associated with the circuit model proposed in the previous section. Our viscoelastic model expressed by Eq. (3.1) (to be explained in detail in the Section 3.1) has the same form as the one in ref. [19]. In ref. [19], the authors studied the bending behavior of a Nafion IPMC one end of which was horizontally clamped with a pair of electrode and the other end of it 15 mm away from the clamping point was placed on the stage of balance as illustrated in Fig. 14. A voltage applied on the Nafion IPMC induced the bending in the anode direction, and the authors made measurements of the time course of Nafion IPMC shape evolution and simultaneously of time course of blocking force it generated recorded by the precision balance (hereafter the bending test condition illustrated in Fig. 14 is called “constraint bending” in contrast to the free bending). The experimental data of the blocking force and the shape evolution of the Nafion IPMC led to the computational derivation of the time-dependent Young’s modulus of the Nafion IPMC.

For explaining the free bending behavior of a CMV IPMC by using viscoelastic theory, we needed to obtain the time-dependent data of Young’s modulus of CMV IPMC, too. However, the bending behavior of CMV IPMC in our question is free bending, and it is different

from the condition of constraint bending. Hence, in this work, we further improved the existing viscoelastic model introduced in ref. [19] and obtained the time-dependent Young’s modulus of CMV IPMC in the process of free bending. Then we attempted to explain the free bending behavior of CMV IPMC.

3.1. Viscoelastic model of CMV IPMC

The free bending here means the bending of a CMV IPMC under a rectangular oscillating voltage (amplitude = 1.5 V, frequency = 1/60 Hz), which is clamped with a pair of electrodes just like Fig. 1. The polarity of the applied voltage was reversed at $t = 15$ s and 45 s. When the CMV IPMC exhibits bending under the applied voltage, the force f indicated by arrows in Fig. 15, must be exerted on the CMV IPMC from its inside. More concretely, f represents the force per unit width (1 mm) of the CMV IPMC. The bending behavior of the CMV IPMC can be expected to obey the general law of viscoelastic materials [20]. We put forth a theoretical model by modifying that of ref. [19] and applying it to our cases.

Suppose that the applied voltage is low and the CMV IPMC does not exhibit large deformation in the free bending, which implies that the displacement of x -direction of CMV IPMC is almost 0. Let $y(t,$

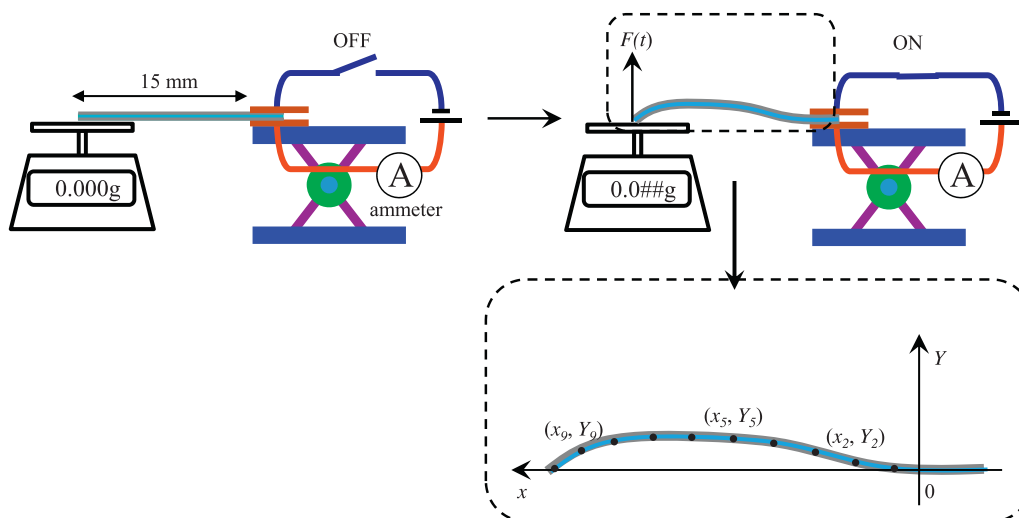


Fig. 14. Experimental setup introduced in ref. [19]. Using this setup, blocking force, $F(t)$, and shape of Nafion IPMC (more concretely, the coordinates of representative points of Nafion IPMC $(x_i(t), Y_i(t))$ were measured as a function of time).

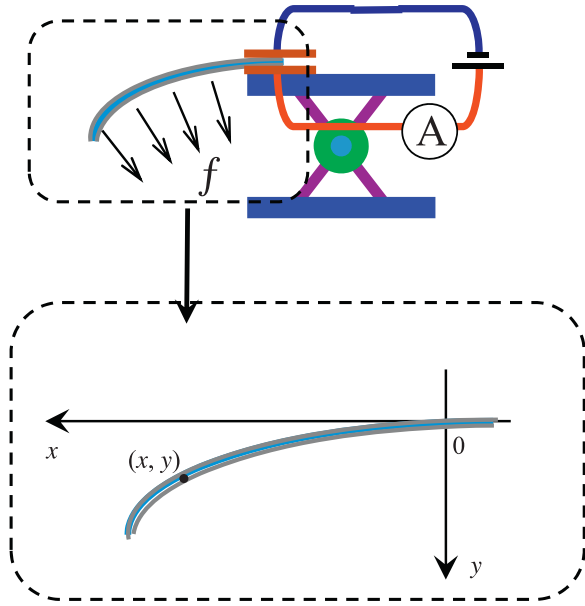


Fig. 15. Fine arrows suggest the induction of force generated from the CMV IPMC inside, which causes the downward bending of IPMC. Coordinate (x, y) of a representative point on a CMV IPMC in the free bending state is shown.

x) be the vertical position of the CMV IPMC beam at given position x at time t as illustrated in Fig. 15. Then a viscoelastic model is represented by

$$\int_0^t E_{fb}(t - \tau) I_m y'''(\tau, x) d\tau + f(t) = 0, \tag{3.1}$$

where $E_{fb}(t)$ is the time-dependent Young's modulus of the CMV IPMC in the free bending and I_m is the moment of inertia of the cross section of the beam. The dot and the prime represent the differentiation with respect to t and x , respectively. The boundary conditions are given by

$$y(t, 0) = 0, \quad y'(t, 0) = 0, \quad y''(t, l) = 0, \tag{3.2}$$

where we denote the length of the CMV IPMC by l . Before moving on to the next step of solving Eq. (3.1), we would like to urge the readers to pay careful attention to Eq. (3.1). The f was earlier defined as the force per unit width (1 mm) of the CMV IPMC, and the width of actual CMV IPMC was 2 mm. Hence, its dimension is [N/mm]. Eq. (3.1) was derived for the CMV IPMC whose width was the same as the unit width of 1 mm. Namely, we considered a beam model of CMV IPMC, 20 mm length \times 1 mm width \times 120 μ m thickness, for deriving Eq. (3.1). Therefore $f(t)$ in Eq. (3.1) represents not $f(t)$ [N/mm] but $f(t)$ [N] given by $f(t)$ [N/mm] \times 1 [mm] = $f(t)$ [N].

By solving Eq. (3.1) under the conditions Eq. (3.2) with respect to x , the displacement $y(t, x)$ can be represented by

$$y(t, x) = \frac{u(t)}{2I_m} (lx^2 - \frac{1}{3}x^3), \tag{3.3}$$

where $u(t)$ is a solution of

$$\int_0^t E_{fb}(t - \tau) \dot{u}(\tau) d\tau = f(t). \tag{3.4}$$

For solving Eq. (3.4) with respect to $u(t)$, it is necessary to obtain $E_{fb}(t)$ and $f(t)$. For deriving $E_{fb}(t)$, we investigated the constraint bending of CMV IPMC first. The coordinates $(x_i, Y_i(t))$ representing the shape evolution of CMV IPMC in the constraint bending state and the blocking force $F(t)$ the CMV IPMC generated (see Fig. 14) were obtained by carrying out the same experiment explained in ref. [19]. It enables us to theoretically estimate the

time-dependence of the Young's modulus, $E_{cb}(t)$, of CMV IPMC in the constraint bending state. By the use of $E_{cb}(t)$, we derived $E_{fb}(t)$ of the CMV IPMC in the process of free bending. The derivation process of $E_{fb}(t)$ and $f(t)$ as well as $E_{cb}(t)$ is described in the next section.

3.2. Derivation of $E_{fb}(t)$ and $f(t)$

Employing the experimental and theoretical techniques described in ref. [19], we first obtain the time-dependent $E_{cb}(t)$ of a CMV IPMC in the constraint bending state. It is detailed below.

One end of the CMV IPMC was horizontally clamped with a pair of electrodes. The other end of the CMV IPMC was placed on the stage of balance as illustrated in Fig. 14. Once constant 1.5 V was imposed on the CMV IPMC, it tended to bend downward. Hence, the tip force was exerted on the stage of precision balance, and the precision balance recorded the blocking force F as a function of time. At the same time the CMV IPMC deforms, and vertical displacement of ten representative points on the surface of CMV IPMC in the constraint bending state, denoted by $Y_i(t)$ at x_i ($i = 1-10$), were measured with a 2-D laser displacement sensor as a function of time, where all x_i are constant, independent of time. According to the formula (12) given in ref. [19], $E_{cb}(t)$ can be theoretically calculated by Eq. (3.5):

$$\hat{E}_{cb}(p) = \frac{2\hat{F}(p)l}{3p\hat{\kappa}(p)I_m}, \tag{3.5}$$

where $\kappa(t)$ denotes the curvature of CMV IPMC at the left end of the CMV IPMC, and the wedge “ $\hat{\cdot}$ ” represents the Laplace transformation, generally defined by

$$\hat{h}(p) = \int_0^\infty h(t)e^{-pt} dt$$

for a function $h(t)$. Actually, $Y(t, x)$ and $\kappa(t)$ have to satisfy

$$Y(t, x) = \frac{\kappa(t)}{4l} x^2 (l - x) \tag{3.6}$$

for any $0 < x < l$.

From these formulas, it is clear that making measurements of the time course of blocking force and the shape evolution are necessary for estimating the Young's modulus. We attempted to estimate the Laplace transformation of $F(t)$ and $\kappa(t)$ as described next: Fig. 16(a) shows the time dependence of the blocking force, $F(t)$, (normalized by the width of CMV IPMC). The experimental data shows approximately linear relationship. Using the data of CMV IPMC shape evolution – the coordinate sets of representative points on the CMV IPMC $(x_i, Y_i(t))$ (see Fig. 15) –, $\kappa(t)$ was calculated by the least squares method shown in ref. [19], and it is shown in Fig. 16(b). Here we assume that the $F(t)$ and the $\kappa(t)$ are given by a simple model as below, where κ_0, κ_1, F_0 and F_1 were obtained by applying the least squares method the experimental data shown in Fig. 16(a) and (b), respectively.

$$\kappa(t) = \kappa_0 + \kappa_1 t \tag{3.7}$$

$$\kappa_0 = 0.00268 \quad \kappa_1 = 0.00011$$

$$F(t) = F_0 + F_1 t. \tag{3.8}$$

$$F_0 = 0.0856 \quad F_1 = 0.00499$$

The Laplace transformations of $F(t)$ and $\kappa(t)$ are explicitly given by

$$\hat{F}(p) = \frac{F_0}{p^2} + \frac{F_1}{p}, \quad \hat{\kappa}(p) = \frac{\kappa_0}{p^2} + \frac{\kappa_1}{p}. \tag{3.9}$$

By substituting these functions into Eq. (3.5) and applying the inverse Laplace transformation, the Young's modulus $E_{cb}(t)$ is

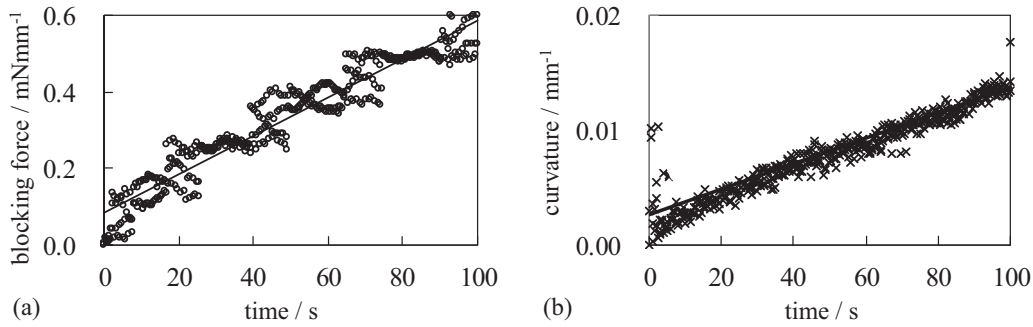


Fig. 16. (a) Time course of blocking force (normalized by the width of CMV IPMC) the CMV IPMC generated under 1.5 V constant applied voltage open circle: experimental linear line: fitting linear line. (b) Time course of the CMV IPMC bending curvature under 1.5 V constant applied voltage × mark: experimental linear line: fitting linear line.

explicitly represented by:

$$E_{cb}(t) = \frac{2l}{3l_m} \left(\frac{F_1}{\kappa_1} + \left(\frac{F_0}{\kappa_0} - \frac{F_1}{\kappa_1} \right) e^{-\frac{\kappa_1}{\kappa_0}t} \right) = 3.15 - 0.937e^{-0.0409t}. \tag{3.10}$$

Eq. (3.10) implies that the Young’s modulus $E_{cb}(t)$ increases monotonically and approaches 3.15 GPa as time grows, which means that the CMV IPMC becomes harder and harder. This result is different from that of the Nafion IPMC in ref. [19], where it was reported that the Young’s modulus estimated for the Nafion IPMC first increases with time till it reaches the maximal peak at a certain time, and eventually decreases as time passes. Hence, Eq. (3.10) indicates the particular feature of the CMV IPMC. However, we cannot use Eq. (3.10) as is. The behavior of CMV IPMC in the free bending state under oscillating voltage is in our question. Since Eq. (3.10) represents $E_{cb}(t)$ in the constraint bending state under constant voltage, it is not applicable for explaining the behavior of the free bending CMV IPMC. It is necessary to find an alternative method of estimating $E_{fb}(t)$. For the purpose of finding out a method of estimating $E_{fb}(t)$, we obtained the relationship E_{cb} vs. Q first, where Q represents the total charge imposed on the CMV IPMC per its unit surface area in the constraint bending state. E_{cb} vs. Q was obtained by the following procedure: In the experiment for obtaining Fig. 16, the current I flowing through the CMV IPMC was measured as a function of time. We numerically calculated the total charge $Q(t)$ imposed on the CMV IPMC by $Q(t_j) = \sum I(t_j)(t_j - t_{j-1})$ ($j = 1, 2, 3, \dots, N$, and we denote $t_0 = 0$ s and $t_N = 100$ s) for obtaining Q vs. t . Since we could obtain Q vs. t here, and already we obtained E_{cb} vs. t by Eq. (3.10), E_{cb} was associated with Q so as to resulting in E_{cb} vs. Q shown in Fig. 17.

Since it has been repeatedly reported that the redox reaction $Ag \leftrightarrow Ag_2O$ was induced on the surface of Selemion CMV-based IPMC, which was virtually the same as CMV IPMC, in the process

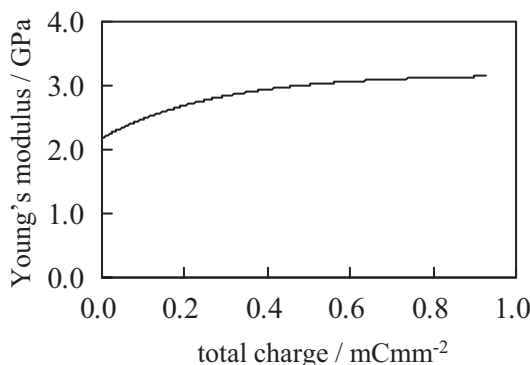


Fig. 17. Young’s modulus (E_{cb}) vs. Total charge imposed on the CMV IPMC.

of its bending [10–12], and it was strongly speculated that the IPMC Young’s modulus had intimate correlation to the creation and vanishing of Ag and Ag_2O [21]. Previously it was experimentally confirmed that the quantity of Ag_2O formed on the IPMC surface was almost proportional to the total charge imposed on the IPMC [22]. Hence, it is speculated that E_{fb} is charge-dependent. Judging from this empirical speculation and the shape of curve representing E_{cb} vs. Q shown in Fig. 17, we put forth Eq. (3.11) as a general expression of Young’s modulus of CMV IPMC, which means Eq. (3.11) represents the CMV IPMC Young’s modulus regardless of the experimental condition the CMV IPMC is in. Appropriately choosing parameters in Eq. (3.11) results in a curve resembling to the diagram Fig. 17.

$$E(q_1, q_2) = e_0 + e_1(1 - e^{-\alpha q_1}) + e_1(1 - e^{-\alpha q_2}). \tag{3.11}$$

Eq. (3.11) is a function of charge, q_1 and q_2 , instead of a function of time. The q_1 represents the charge quantity passing through the bottom surface, involved in the redox reaction $Ag \leftrightarrow Ag_2O$, while q_2 represents the charge quantity passing through the top surface, involved in the redox reaction $Ag \leftrightarrow Ag_2O$. The e_0 represents the Young’s modulus of intact CMV IPMC. The second term and third term of Eq. (3.11) represent the variation of Young’s modulus of CMV IPMC caused by the redox reaction of silver layers of bottom and top surfaces, respectively. The α is the decay rate associated with increase/decrease of Ag_2O quantity on the individual surfaces of a CMV IPMC. Now, we will estimate the parameters in Eq. (3.11).

As described earlier, $E_{cb}(t)$ is expressed by Eq. (3.10), when the constant voltage is imposed on the CMV IPMC. In this experiment illustrated in Fig. 14, a constant voltage of 1.5 V continued being imposed on the CMV IPMC, and no polarity change was performed. Hence, Ag_2O kept on emerging on the bottom surface by the oxidation of Ag , while the Ag on top layer exhibited no response to the applied voltage. What we would like to mention here is that if some

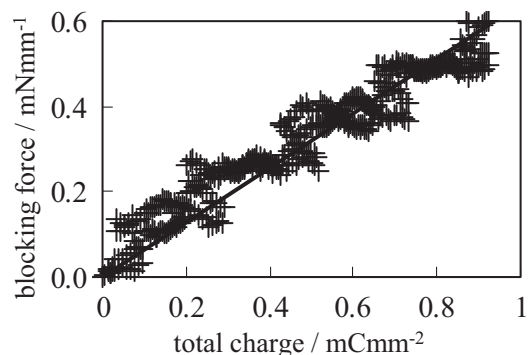


Fig. 18. Blocking force CMV IPMC generated vs. total charge imposed on the CMV IPMC.

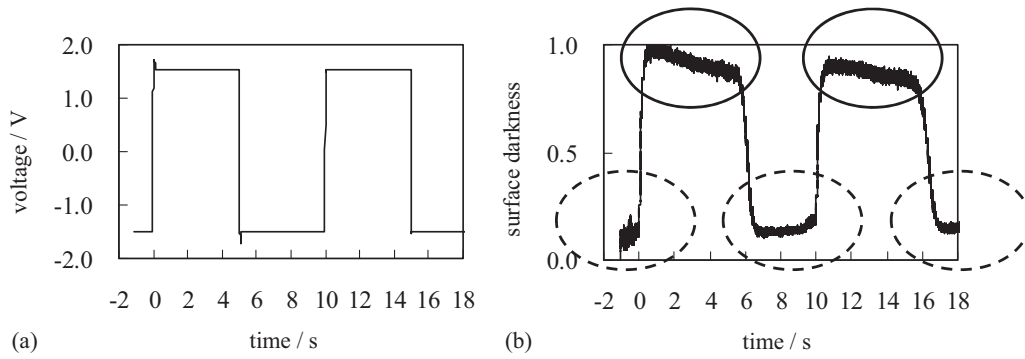


Fig. 19. (a) Wave form of voltage imposed on the CMV IPMC (b) Surface darkness index of CMV IPMC vs. time.

Ag_2O existed on the top surface, undoubtedly it would be reduced into Ag, but actually not. By the definition of q_1 and q_2 described earlier, these charges represent only the charge involved in the redox reaction of $\text{Ag} \leftrightarrow \text{Ag}_2\text{O}$. Hence q_2 was identical to 0. Thus the parameters in Eq. (3.11) are estimated as $e_0 = 2.18$, $e_1 = 0.999$ and $\alpha = 3.59$. Hence, we have obtained the Young's modulus for the oscillatory free bending IPMC as a function of charge. Namely, $E_{fb} = E(q_1, q_2)$. One might argue that this viscoelastic model treats whole current so that it is involved in the redox reaction, although not all the charge flowing through the CMV IPMC is involved in the redox reaction of $\text{Ag} \leftrightarrow \text{Ag}_2\text{O}$ according to the circuit model. Concerning the circuit model, in fact, the current flowing through r_s and C_s (see Fig. 5(a)) is not related to the redox reaction of $\text{Ag} \leftrightarrow \text{Ag}_2\text{O}$. Since the current flowing through r_s and C_s is virtually negligible, the viscoelastic model is consistent with the circuit model.

Next we would like to derive the concrete form of f in the free bending state. As described above, it is also difficult to measure it experimentally. According to ref. [21], it was observed that the blocking force by a Selemion CMV-based IPMC (same as a CMV IPMC) was roughly proportional to the charge imposed on the CMV IPMC. Furthermore, based on the basic concept of strength of materials, f is the same as the blocking force. Hence, f could be assumed to be proportional to the charge imposed on the CMV IPMC as given by Eq. (3.12)

$$f = K(q_1 - q_2), \quad (3.12)$$

where q_1 and q_2 are the same charges as in Eq. (3.11).

Now we estimated K in Eq. (3.12). As described earlier, the blocking force in Fig. 16(a) was measured along with the current I as a function of time. Those experimental data – time course of blocking force (same as f) shown in Fig. 16(a) and time course of current I – were rearranged into the blocking force vs. total charge imposed on the CMV IPMC as in Fig. 18. As is the case with the procedure of determining the parameters of Eq. (3.11), q_2 is zero. Linear line shown in Fig. 18 is a fitting linear line of blocking force vs. total charge imposed on the CMV IPMC. The slope of this linear fitting line is K and is 0.639.

3.3. Prediction of bending behavior based on the viscoelastic model

In the previous section, we derived formulas of E_{fb} and f both as a function of charge. Then we attempt to solve Eq. (3.4) with respect to u as analytically as possible. In order to verify the validity of our viscoelastic model, we check up if u of our viscoelastic model can reproduce the oscillatory bending behavior, for example, Fig. 9(b-1).

Firstly, we need explicit forms of the charge behavior. Since the current was measured experimentally and the charge can be easily obtained by integrating the current with respect to time,

we propose a model of the current behavior. Based on the circuit model introduced in the section 2, it was assumed that the current takes the forms represented by

$$\begin{aligned} I_1(t) &= I_{10} + I_{11}e^{-\beta_{11}t} + I_{12}e^{-\beta_{12}t} & 0 \leq t \leq 15 \text{ s}, \\ I_2(t) &= I_{20} + I_{21}e^{-\beta_{21}(t-15)} + I_{22}e^{-\beta_{22}(t-15)} & 15 \leq t \leq 45 \text{ s}, \\ I_3(t) &= I_{30} + I_{31}e^{-\beta_{31}(t-45)} + I_{32}e^{-\beta_{32}(t-45)} & 45 \leq t \leq 75 \text{ s}. \end{aligned} \quad (3.13)$$

$$i = 1, 2, 3; j = 0, 1, 2; k = 1, 2 \text{ for } I_i, I_{ij} \text{ and } \beta_{ik}.$$

By the procedure described in Appendix C, all the parameters are given by Eq. (3.14).

$$\begin{aligned} I_{10} &= 0.00435, & I_{11} &= 0.0103, & I_{12} &= 0.0104, & \beta_{11} &= 11.5, & \beta_{12} &= 1.88, \\ I_{20} &= -0.00427, & I_{21} &= -0.042, & I_{22} &= -0.00264, & \beta_{21} &= 1.45, & \beta_{22} &= 0.167, \\ I_{30} &= 0.00443, & I_{31} &= 0.0173, & I_{32} &= 0.031, & \beta_{31} &= 12.7, & \beta_{32} &= 0.418. \end{aligned} \quad (3.14)$$

The current is positive from $t=0$ s to 15 s and from 45 s to 75 s, while it is negative from $t=15$ s to 45 s.

Electrical properties of CMV IPMC are quite sensitive to the environmental humidity. Although we carried out all the experiments by maintaining the environmental absolute humidity at 9 gm^{-3} , it was practically impossible to achieve the perfect 9 gm^{-3} absolute humidity environment. Unfortunately, slight deviation of say 0.5 gm^{-3} from the absolute humidity from of 9 gm^{-3} can cause large change of some properties of CMV IPMC such as current and bending curvature. However, basically the bending curvature vs. charge relationship of CMV IPMC exhibits similar behavior to the diagram shown in Fig. 9(b-1), even though the slight deviation of absolute humidity happens, as long as the environmental absolute humidity is low enough (empirically less than 10 gm^{-3}). More concretely, the following characteristics (I)–(III) are observed in the low absolute humidity environment, even though the absolute humidity slightly

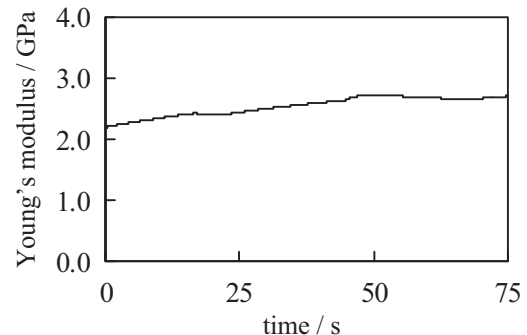


Fig. 20. Time dependence of Young's modulus (E_{fb}) of CMV IPMC.

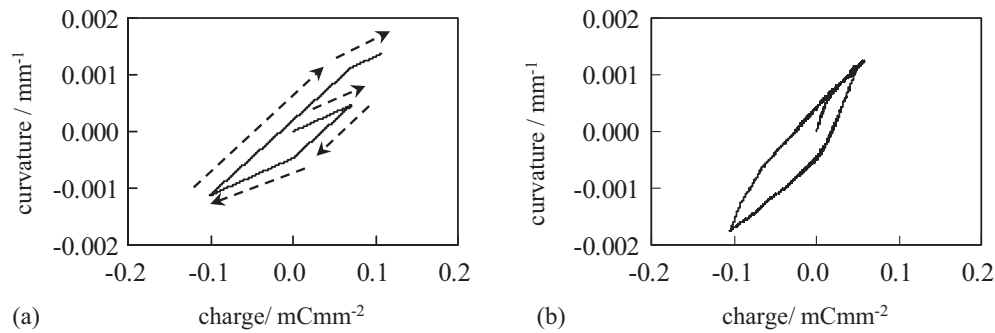


Fig. 21. Curvature vs. Charge of CMV IPMC from $t=0$ s through 75 s (a) Theoretical prediction by viscoelastic model, where the arrows suggest the time progression (b) Experimental result.

deviates from the desired. In fact, the diagram in Fig. 9(b-1) bears all the three characteristics below, (I)–(III).

- (I) Diagram of bending curvature vs. charge takes a very long parallelogram form (it roughly looks a single straight line).
- (II) If the diagram is approximated by a single straight line as described in (I) above, its slope usually takes a particular value not far different from the order of 0.01 mC^{-1} .
- (III) Time direction of diagram of bending curvature vs. charge is clockwise (though it often turns counter-clockwise in high absolute humidity environment).

From Eqs. (3.13) and (3.14), Eq. (3.15) was obtained (see Appendix C).

$$\begin{aligned} Q_1(t) &= 0.00643 + 0.00435t - 0.0009e^{-11.5t} - 0.00553e^{-1.88t}, \\ Q_2(t) &= 0.0267 - 0.00427(t - 15) + 0.0291e^{-1.45(t-15)} + 0.0158e^{-0.167(t-15)}, \\ Q_3(t) &= -0.0259 + 0.00443(t - 45) - 0.00137e^{-12.7(t-45)} - 0.074e^{-0.418(t-45)}. \end{aligned} \quad (3.15)$$

Although the explicit forms of the charge Eq. (3.15) can be completely determined by experimental data, exactly speaking, it is impossible to estimate q_1 and q_2 in Eqs. (3.11) and (3.12) only by the experimental data, since not all the experimentally measured charge was involved in the redox reaction $\text{Ag} \leftrightarrow \text{Ag}_2\text{O}$. Namely, according to the circuit model, a certain quantity of charge flowed through r_s and C_s , which was not involved in the redox reaction at all. But as described earlier repeatedly, the quantity of such charge was usually negligibly small. Therefore, we hypothesized that the whole charge was involved in the redox reaction unless specifically commented. Hence, the quantity of Ag oxidized at anode surface was the same as that of Ag created by the reduction of Ag_2O . This speculation is supported by the experimental observation of CMV IPMC surface color below.

Rectangular oscillating voltage shown in Fig. 19(a) was imposed on the CMV IPMC. Darkness of the CMV IPMC bottom surface was monitored, during the voltage application, by the use of high speed microscope VW-9000 (Keyence, Osaka, Japan). When the voltage was positive, the bottom surface was anode, and when the voltage was negative, the bottom surface was cathode. Fig. 19(b) shows the time dependence of darkness index of CMV IPMC bottom surface, where the darkness index was normalized by the maximal darkness index. Dark surface suggests the creation of Ag_2O by the oxidation of Ag, because Ag_2O is black. Bright surface suggests the creation of Ag by the reduction of Ag_2O , because Ag is white. Maximal darkness index was quantitatively repeatable as clearly indicated by solid ovals in Fig. 19(b), while minimal darkness index was quantitatively repeatable, too, as indicated by dashed ovals. This experimental observation suggests that the whole Ag_2O created by the Ag

oxidation was reduced into Ag again and whole Ag created by the Ag_2O reduction was oxidized into Ag_2O . This result is further interpreted as impose of the a certain quantity of charge, say δ [Coulomb] which is involved in the redox reaction, on one surface of CMV IPMC indicates that quantity of charge $-\delta$ [Coulomb] is involved in the redox reaction on the opposite surface of the CMV IPMC. Considering the discussion so far, we derived the explicit forms of q_1 and q_2 at arbitrary time, where the detail is described in Appendix D.

Substituting the functions q_1 and q_2 (see Appendix D) defined above into the Eq. (3.11), we obtained the time-dependent Young's modulus $E_{fb}(t)$, which is shown in Fig. 20. Taking a close look at this diagram reveals that the Young's modulus exhibits a bit wavy form as expected but approximately constant. In order to simplify the process of solving Eq. (3.4) analytically, we consider $E_{fb}(t)$ as constant and takes as the value of the Young's modulus of CMV IPMC, which was calculated as $E_0 = 2.54 \text{ GPa}$. Then Eq. (3.4) is rewritten into

$$E_0 u(t) = f(t), \quad (3.16)$$

where the force $f(t)$ was obtained by the direct substitutions of the functions q_1 and q_2 into Eq. (3.12).

As a result, we could theoretically predict the relationship between the free bending CMV IPMC curvature and charge imposed on the CMV IPMC by the viscoelastic model. The theoretical prediction is shown in Fig. 21(a) along with typical experimental result shown in Fig. 21(b) obtained by the use of experimental setup for viscoelastic model study. Though the theoretical prediction a bit underestimated the curvature, it still can be said that the curvature vs. charge was successfully predicted quantitatively. Furthermore, theoretical result agrees with the characteristics (I)–(III) introduced earlier. We have not found yet the reason of underestimate of curvature by the theoretical prediction, but we strongly suspect that it is due to the experimental error in making measurement of blocking force described in the Section 3.2. The blocking force was quite small and its measurement was so critical. Even slight environmental air flow causes undesired noise to the precision balance.

4. Conclusions

The bending behavior of CMV IPMC (Selemon CMV-based IPMC) was quantitatively well reproduced employing circuit model. Especially we would like to emphasize that the Faradaic and non-faradaic current were found to have distinguished influence on the bending induction. Employing a concept of the circuit model, viscoelastic analysis on the bending behavior of CMV IPMC was carried out. The computational result obtained by the viscoelastic model successfully predicted the experimental bending behavior of CMV IPMC. Hence, the appropriateness of the circuit model was validated by a concept of physics, viscoelasticity.

It gives the circuit model a certain level of usefulness for predicting the bending behavior of IPMC.

To our best knowledge, no one has succeeded in quantitatively predicting the far future bending behavior of IPMC. Therefore, prediction of far future bending behavior of CMV IPMC is our next challenging task.

Acknowledgment

We would like to express our gratitude to Mr. Yoshihisa Kinoshita (KEYENCE) for his technical assistance to conduct this research. This research was conducted under the financial support of the Ministry of Education, Science, Sports and Culture, Grant-in-Aid for Scientific Research (C), 24560291,2012.

Appendix A.

We derived the circuit equations about the circuit shown in Fig. 10 as below:

$$I = I_s + I_l + I_R \tag{A.1}$$

$$I_r = I_l + I_R \tag{A.2}$$

$$V = \frac{Q_s}{C_s} + I_s r_s \tag{A.3}$$

$$\frac{dQ_s}{dt} + I_s \tag{A.4}$$

$$V = \frac{Q_l}{C_l} + I_r r_l \tag{A.5}$$

$$\frac{dQ_l}{dt} + I_l \tag{A.6}$$

$$V = I_R R + I_r r_l \tag{A.7}$$

$$\frac{Q_l}{C_l} + I_R R \tag{A.8}$$

Solving the above equations resulted in Eq. (2.1) where Q_s and Q_l were both zero at $t=0$ s.

Appendix B.

We derived the circuit equations after $t'=0$ about the circuit shown in Fig. 10 as below:

$$V' = \frac{Q'_s}{C'_s} + \frac{dQ'_s}{dt'} r'_s \tag{B.1}$$

$$V' = \frac{Q'_l}{C'_l} + \frac{dQ'_l}{dt'} r'_l + \frac{Q'_l}{R' C'_l} r'_l \tag{B.2}$$

These equations were solved for $Q'_s(t')$ and $Q'_l(t')$, where $V' = -1.5$ V, $Q'_s(t'=0\text{s}) = Q_s^T$, and $Q'_l(t'=0\text{s}) = Q_l^T$. Following equations were derived:

$$Q'_s(t') = Q'_s \left[1 - \exp\left(-\frac{t'}{\tau'_s}\right) \right] + Q_s^T \exp\left(-\frac{t'}{\tau'_s}\right) \tag{B.3}$$

where $Q'_s = C'_s V'$ ($V' = -1.5$ V), $t' = t - T$ and $\tau'_s = r'_s C'_s$

$$Q'_l(t') = Q'_l \left[1 - \exp\left(-\frac{t'}{\tau'_l}\right) \right] + Q_l^T \exp\left(-\frac{t'}{\tau'_l}\right) \tag{B.4}$$

where $Q'_l = \frac{R'}{r'_l + R'} C'_l V'$ ($V' = -1.5$ V), $t' = t - T$ and $\tau'_l = \frac{C'_l r'_l R'}{r'_l + R'}$

Next we derived an equation of $I'(t')$ just like Eq. (2.4) as follows:

$$I'_s(t') = \frac{d}{dt'} Q'_s(t') = \frac{Q'_s}{\tau'_s} \exp\left(-\frac{t'}{\tau'_s}\right) - \frac{Q_s^T}{\tau'_s} \exp\left(-\frac{t'}{\tau'_s}\right) \tag{B.5}$$

$$I'_l(t') = \frac{d}{dt'} Q'_l(t') = \frac{Q'_l}{\tau'_l} \exp\left(-\frac{t'}{\tau'_l}\right) - \frac{Q_l^T}{\tau'_l} \exp\left(-\frac{t'}{\tau'_l}\right) \tag{B.6}$$

$$I'_R(t') = \frac{Q'_l}{R' C'_l} = \frac{q'_l}{R' C'_l} + \frac{Q_l^T - q'_l}{R' C'_l} \exp\left(-\frac{t'}{\tau'_l}\right) \tag{B.7}$$

Solving the above equations resulted in Eq. (2.7).

Appendix C.

We estimated all the parameters in Eq. (3.13) by the following procedure: Owing to the Eq. (3.13), the charge formulas are given as simple expressions as below:

$$\begin{aligned} Q_1(t) &= I_{10}t + \frac{I_{11}}{\beta_{11}}(1 - e^{-\beta_{11}t}) + \frac{I_{12}}{\beta_{12}}(1 - e^{-\beta_{12}t}) & 0 \text{ s} \leq t \leq 15 \text{ s,} \\ Q_2(t) &= Q_1(15) + I_{20}(t - 15) + \frac{I_{21}}{\beta_{21}}(1 - e^{-\beta_{21}(t-15)}) + \frac{I_{22}}{\beta_{22}}(1 - e^{-\beta_{22}(t-15)}) & 15 \text{ s} \leq t \leq 45 \text{ s,} \\ Q_3(t) &= Q_2(45) + I_{30}(t - 45) + \frac{I_{31}}{\beta_{31}}(1 - e^{-\beta_{31}(t-45)}) + \frac{I_{32}}{\beta_{32}}(1 - e^{-\beta_{32}(t-45)}) & 45 \text{ s} \leq t \leq 75 \text{ s.} \end{aligned} \tag{C.1}$$

All the parameters in Eq. (C.1) are employed in Eq. (3.13). Since the charge changes continuously, $Q_2(15) = Q_1(15)$ and $Q_3(45) = Q_2(45)$, respectively. We estimated all the parameters in Eq. (C.1) by the use of the current experimentally obtained by applying the rectangular oscillating voltage (amplitude = 1.5 V, frequency = 1/60 Hz) on a CMV IPMC in the free bending state. Employing the Newton method, the parameters in Eq. (C.1) (or in (3.13)) are estimated as given by Eq. (3.14).

Here, we have to make a comment that we did not use the experimental data of current shown in Fig. 11, which was used in the circuit model study, for obtaining the results given by Eq. (3.14). Instead of it, we chose to use the current data obtained by using the experimental setup for viscoelastic model study (data not shown in this paper). It is due to the following reason: Since our experimental setup employed for viscoelastic model study was not exactly same as that employed for circuit model study, we thought that it was better to use the current data obtained by employing the setup for the viscoelastic model study, as long as we performed viscoelastic model study. But the relationship curvature vs. charge was basically the same as in Fig. 9(b-1) regardless of the experimental setup employed.

Appendix D.

Explicit form of q_1 and q_2 at arbitral time were derived by the following discussion:

It is clear that q_1 and q_2 for $0 \text{ s} \leq t \leq 15 \text{ s}$ are given by the following equations:

$$q_1 = Q_1(t) \quad (\text{D.1})$$

$$q_2 = 0 \quad (\text{D.2})$$

After the polarity of the applied voltage is reversed, the following two equations are valid until q_1 becomes 0. Hence, the following two equations are derived:

$$q_1 = Q_2(t) \quad (\text{D.3})$$

$$q_2 = Q_1(15) - Q_2(t) \quad (\text{D.4})$$

Since $Q_2(t)$ is equal to 0 at $t = 22.3 \text{ s}$ from the Eq. (C.1), $q_1 = 0$ and $q_2 = Q_1(15)$ at $t = 22.3 \text{ s}$. Since reduction of Ag_2O on a surface stops at $t = 22.3 \text{ s}$, all energy is consumed only for oxidization of Ag on the surface of the other side, which implies that $q_2 = Q_1(15) - Q_2(t)$ from $t = 22.3 \text{ s}$ to 45 s .

$$q_1 = 0 \quad (\text{D.5})$$

$$q_2 = Q_1(15) - Q_2(t) \quad (\text{D.6})$$

By the same argument, following four equations were derived:

$$q_1 = Q_3(t) - Q_2(45) \quad (\text{D.7})$$

$$q_2 = Q_1(15) - Q_3(t) \quad (\text{D.8})$$

where the above two equations are valid for $45 \text{ s} \leq t \leq 67 \text{ s}$.

$$q_1 = Q_3(t) - Q_2(45) \quad (\text{D.9})$$

$$q_2 = 0 \text{ at } t = 67 \text{ s and onward} \quad (\text{D.10})$$

where the above two equations are valid for $67 \text{ s} \leq t \leq 75 \text{ s}$.

References

- [1] K. Oguro, Y. Kawami, H. Takenaka, Bending of an ion-conducting polymer film–electrode composite by an electric stimulus at low voltage, *Trans. J. Micro-mach. Soc.* 5 (1992) 27–30.
- [2] K. Oguro, K. Asaka, H. Takenaka, Polymer film actuator driven by low voltage, in: *Proceedings of 4th International Symposium on Micro Machine and Human Science*, 1993, pp. 39–40.
- [3] K. Asaka, K. Oguro, Y. Nishimura, M. Mizuhara, H. Takenaka, Bending of polyelectrolyte membrane–platinum composite by electric stimuli I, response characteristics to various waver forms, *Polym. J.* 27 (1995) 436–440.
- [4] K. Salehpoor, M. Shahinpoor, M. Mojarrad, Linear and platform type robotic actuators made from ion-exchange membrane–metal composites, *Proc. SPIE Smart Mater. Struct.* 3040 (1997) 192–198.

- [5] Y. Bar-Cohen, T. Xue, M. Shahinpoor, K. Salehpoor, J. Simpson, J. Smith, Low-mass muscle actuators using electroactive polymers (EAP), in: *Proc. SPIE Smart Mater. Struct.*, 1998, Paper-No. 324–32.
- [6] M. Uchida, M. Taya, Solid polymer electrolyte actuator using electrode reaction, *Polymer* 42 (2001) 9281–9285.
- [7] S. Nemat-Nasser, Micromechanics of actuation of ionic polymer–metal composites, *J. Appl. Phys.* 92 (5) (2002) 2899–2915.
- [8] S. Nemat-Nasser, Y. Wu, Comparative experimental study of ionic polymer–metal composites with different backbone ionomers and in various cation forms, *J. Appl. Phys.* 93 (9) (2003) 5255–5267.
- [9] H. Tamagawa, F. Nogata, Bending response of dehydrated ion exchange polymer membranes to the applied voltage, *J. Membr. Sci.* 243 (2004) 229–234.
- [10] H. Tamagawa, F. Nogata, Atomic structural change of silver-plating layers on the surfaces of Selemion, resulting in its excellent bending controllability, *Sens. Actuators B: Chem.* 114 (2006) 781–787.
- [11] H. Tamagawa, F. Nogata, Charge and water in need for the precise control of Selemion bending, *Sens. Actuators B: Chem.* 121 (2007) 469–475.
- [12] H. Tamagawa, K. Kikuchi, M. Sasaki, Quantity of Ag_2O versus Ag-plated Selemion CMV curvature, in: *Asia Pacific Symposium of Applied Electromagnetics and Mechanics*, Kuala Lumpur, Malaysia, July 28–30, Electrical and Electronic Engineering, 2010, pp. 252–253.
- [13] W. Lin, *Mater. Gifu University*, 2012 (Thesis).
- [14] H. Tamagawa, T. Watanabe, A. Abe, K. Yagasaki, J.-Y. Jin, Influence of metal plating treatment on the electric response of Nafion, *J. Mater. Sci.* 38 (2003) 1039–1044.
- [15] C. Bonomo, L. Fortuna, P. Giannone, S. Graziani, A circuit to model the electrical behavior of an ionic polymer–metal composite, *IEEE Trans. Circuits Syst. I Reg. Papers* 53 (2006) 338–350.
- [16] K. Takagi, T. Osada, K. Asaka, Y. Hayakawa, Z.-W. Luo, Distributed parameter system modeling of IPMC actuators with the electro-stress diffusion coupling theory, in: *Proceedings of SPIE 7287 Electroactive Polymer Actuators and Devices (EAPAD)*, SPIE, 2009, 72871Q.1–72871Q.12.
- [17] Z. Chen, D.R. Hedgpeeth, X. Tan, A nonlinear, control-oriented model for ionic polymer–metal composite actuators, *Smart Mater. Struct.* 18 (2009) 055008.
- [18] K. Park, Characterization of the solvent evaporation effect on ionic polymer–metal composite sensors, *J. Korean Phys. Soc.* 59 (2011) 3401–3409.
- [19] K. Yagasaki, H. Tamagawa, Experimental estimate of viscoelastic properties for ionic polymer–metal composites, *Phys. Rev. E* 70 (2004) 052801.
- [20] J.D. Ferry, *Viscoelastic Properties of Polymers*, Wiley, New York, 1960.
- [21] H. Tamagawa, F. Nogata, Dominant factor for the precise bending control of Selemion, *Sens. Actuators B: Chem.* 120 (2006) 19–24.
- [22] H. Tamagawa, K. Kikuchi, M. Sasaki, Quantity of Ag_2O created vs. Ag-plated Selemion CMV curvature, *J. Jpn. Soc. Appl. Electromagn. Mech.* 19 (2011) S244–S249.

Biographies

Kota Ikeda obtained PhD from Tohoku University, Japan in 2008. He is a specially appointed lecturer in Meiji University, Japan, and currently involved in the research on pattern formation problems and reaction diffusion equations.

Minoru Sasaki obtained PhD from Tohoku University, Japan in 1985. He is a professor in Gifu University, Japan, and currently involved in the research on robotics and control theory.

Hirohisa Tamagawa obtained PhD from Tokyo Institute of Technology, Japan in 1997. He is an assistant professor in Gifu University in Japan and currently involved in the research on the biomaterials, especially electroactive polymers.